An isolated bipolar DC-DC converter for energy storage integration in marine vessels

Nag, Soumya Shubhra; Satpathi, Kuntal; Ukil, Abhisek; Pou, Josep; Zagrodnik, Michael Adam

2017

Nag, S. S., Satpathi, K., Ukil, A., Pou, J., & Zagrodnik, M. A. (2017). An isolated bipolar DC-DC converter for energy storage integration in marine vessels. IECON 2017 - 43rd Annual Conference of the IEEE Industrial Electronics Society, 6765-6770. doi:10.1109/IECON.2017.8217182

https://hdl.handle.net/10356/100175

https://doi.org/10.1109/IECON.2017.8217182

An Isolated Bipolar DC-DC Converter for Energy Storage Integration in Marine Vessels

Soumya Shubhra Nag[1], Kuntal Satpathi[1], Abhisek Ukil[1], Josep Pou[1], Michael Adam Zagrodnik[2]
[1]School of Electrical and Electronic Engineering, Nanyang Technological University, Singapore
[2]Rolls-Royce Singapore Pte. Ltd., Singapore
{soumya.nag, kuntal001, aukil, j.pou}@ntu.edu.sg, michaeladam.zagrodnik@rolls-royce.com

***Abstract*— Integrated power systems (IPSs) with medium voltage direct current (MVDC) distribution are gaining importance in civil and defense marine vessels as they promise to provide cleaner, more reliable operation of vessels along with reduced fuel consumption. The integration of battery energy storage systems (BESSs) in the MVDC distribution system enables peak shaving of generators, optimal scheduling of generators, and near instantaneous power reserve. In this paper, an isolated bipolar dc-dc converter is presented which interfaces the BESS with the bipolar dc distribution bus. The proposed converter uses high frequency transformer isolation which helps in protecting the BESS against rapid discharge in the event of short circuit faults on the dc bus. Detailed steady-state analysis of the proposed converter is presented in this paper. A closed loop control system is developed in the MATLAB®/Simulink simulation platform which regulates the output of the isolated bipolar converter to its reference value. The dynamic performance of the converter is demonstrated with load variations on both the positive and negative buses. The battery discharge limiting capability is also verified.**

Keywords*— *DC ship; Marine vessel; Bipolar dc-link; MVDC distribution; Isolated converter; Battery energy storage system.

I. INTRODUCTION

Generation and power distribution systems for marine vessels are mostly ac systems. The fuel savings that is realizable with variable speed generators have however led to the increased interest in the application of dc distribution systems in marine vessels. As compared to the fixed speed generators, variable speed diesel generators have been reported to yield fuel savings in the range of 20% [1]. In addition to fuel savings, dc distribution is favourable for the integration of battery energy storage [2], [3] and supply of power for pulsed loads [4]. Furthermore, the operation of the multi-generation system is simplified with the absence of critical phase and frequency synchronisation requirements.

In recent years, fully-electric, battery operated ferries have been brought into service for inter-island passenger transfer [5]-[6]. Following this trend, the naval landing craft, yachts, cruise ships, construction vessels, passenger shuttles, house boats, and many others are expected to take advantage of dc distribution and battery storage in the coming years.

In dc shipboard power systems, the source of electrical power are typically synchronous generators driven by diesel generators. The generators are connected to voltage source converters (VSCs), the output of which forms the dc bus. The dc bus voltage can vary from above 1 kV to 35 kV [7] for MVDC distribution. In small marine vessels, like in dc ferries and cruises, the dc bus voltage is generally maintained at 1000 V to 1500 V [1], [8]-[11]. The dc distribution bus can be unipolar or bipolar type [12]-[14]. However, a bipolar dc bus (±500 V or ±750 V) is useful as it exhibits lower transmission loss (owing to lower current in the return wire), higher reliability, and ability to power different loads at two different voltage levels [12]. The low power loads can be connected between pole to ground (i.e., across 500 V or 750 V terminal) and the high power loads can be connected across the pole to pole (corresponding to 1000 V or 1500 V).

A battery storage system (BESS) can be connected to the dc distribution bus directly or through a bi-directional converter [10]. In the case of direct connection, the voltage of the dc bus is determined by the state of charge (SOC) of the battery bank and hence regulation of the dc bus voltage is not possible. Also, a short circuit fault at the dc bus results in unrestricted flow of discharge current which might be detrimental to the battery storage system. Thus, interfacing the battery storage system through a power electronic converter may be a suitable alternative as this would enable dc bus voltage regulation as well as prevent the battery from rapid discharge in the event of short circuit fault.

In this paper, an isolated bipolar dc-dc converter is presented which can form a bipolar dc bus at its output from a single dc source/battery bank. The converter is also capable of restricting rapid discharge of the battery bank in the event of dc bus short circuit.

The paper is organized as follows. Section II presents the circuit diagram of the proposed converter with its equivalent circuit. The operating principles and steady-state analysis of the converter are presented in Section III. The effect of leakage inductance (of the isolation transformer) on the converter operation and the ability to reduce battery discharge in the event of short circuit fault are also included in Section III. Simulation results are provided in Section IV depicting the closed loop operation of the converter, dynamic performance during load change, and the battery discharge restricting capability during fault. Concluding remarks are presented in Section V.

II. DC DISTRIBUTION SYSTEM WITH PROPOSED ISOLATED BIPOLAR CONVERTER

For battery integrated marine vessels, two approaches are followed [10].

a) The traditional approach is to connect the battery bank to the dc bus through a bi-directional dc-dc converter, as

This work was conducted within the Rolls-Royce@NTU Corporate Lab, supported by the National Research Foundation (NRF) Singapore, under the Corp Lab@University Scheme.

shown in Fig. 1. (a). In this approach, the battery charging involves processing of power through two converters (VSC and bi-directional dc-dc converter) and discharging through one converter (bi-directional dc-dc converter). In the case of short circuit fault at the dc bus, the battery bank can be saved from discharging rapidly if the bi-directional dc-dc converter can isolate the battery from dc bus.

b) The modern dc ferries, however, the battery bank is directly connected at the dc bus which requires a battery bank of similar nominal voltage of the dc bus [10]. In such configurations, the voltage of the dc bus can fluctuate depending on the SOC of the battery bank. Any short circuit fault on the dc bus results in rapid discharge of the battery bank and affects the battery bank lifespan.

The advantages of both schemes can be congregated if the battery bank is placed in between the VSC and a dc-dc converter connected to the dc bus, as shown in Fig. 1 (b). In this scheme, the charging of the battery bank is done through the VSC. The battery bank supplies power to the marine loads (including the propulsion) through the dc bus interfacing dc-dc converter which is uni-directional. Thus, the charging and discharging processes involve power processing through one converter. During short circuit faults at the dc bus, the dc-dc converter can isolate the battery bank from the rest of the distribution network, thus preventing its rapid discharge. The proposed isolated bipolar dc-dc converter, described in the next section, can perform the aforementioned operation.

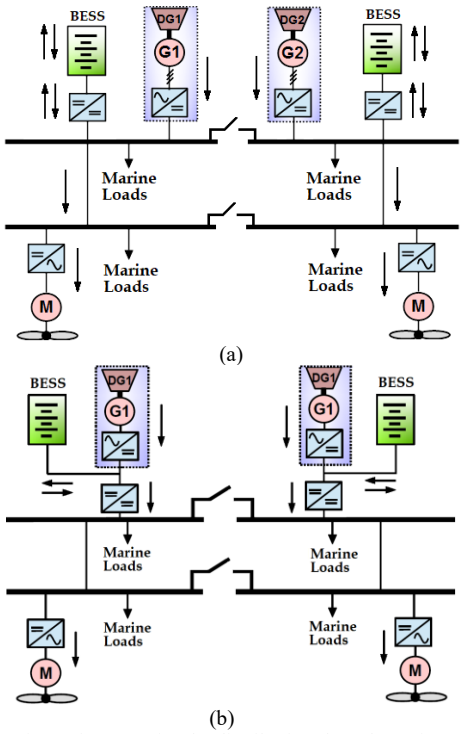

Fig. 1. Integration of BESS in dc distribution based marine vessels: (a) traditional approach and (b) an alternative approach.

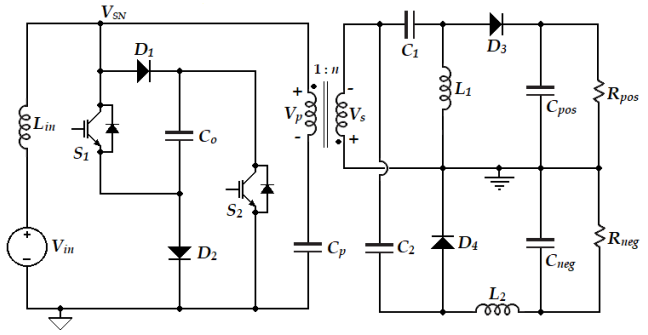

Fig. 2. Circuit schematic of the isolated bipolar dc-dc converter.

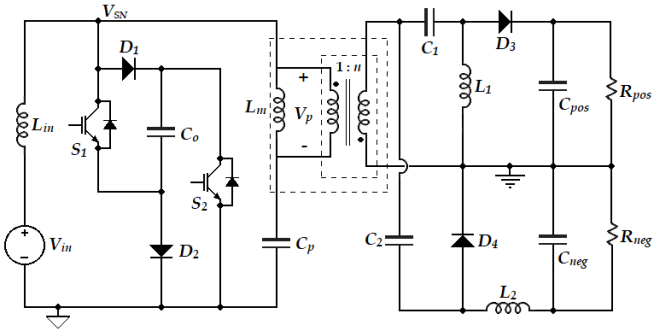

Fig. 3. Schematic diagram of the isolated bipolar dc-dc converter with transformer equivalent circuit.

III. Proposed Isolated Bipolar DC-DC Converter

The circuit diagram of the proposed isolated bipolar dc-dc converter is shown in Fig. 2. The converter has two power stages which are isolated by a high frequency (HF) transformer. The first stage is derived from the current-fed dc-dc bridge structure [15] which produces an AC voltage across the primary side of the HF transformer. The HF transformer has N_p primary and N_s secondary turns with turns-ratio $n=N_s/N_p$. The second stage connects the secondary side of the HF transformer to form a bipolar dc bus.

The HF transformer is replaced by its equivalent circuit model with magnetizing inductance L_m, as shown in Fig. 3. The switches S_1 and S_2 of the converter are turned on and off synchronously. It is assumed that the converter operates in continuous conduction mode (CCM).

IV. Principle of Operation and Steady-State Analysis of the Proposed Converter

A. Operating Princple

The converter operates in two subintervals within a switching cycle. During the first subinterval or D interval ($0 < t < DT_S$), the switches S_1 and S_2 are turned on. The diodes D_1 and D_2 become reverse biased while on the secondary side, diodes D_3, D_4 start conducting. The input inductor current i_{in} increases with slope $(V_{in}+V_c)/L_{in}$ and energy is transferred to the inductor L_{in} from the dc source and the capacitor C_o. The schematic diagram of the proposed converter during the first subinterval (D interval) is shown in Fig. 4 (a). The voltage across the input inductor L_{in} (v_{Lin}), primary and secondary windings of the HF transformer (v_p and v_s, respectively), output side inductors L_1 and L_2 (v_{L1} and v_{L2}, respectively) are given in (1) - (7).

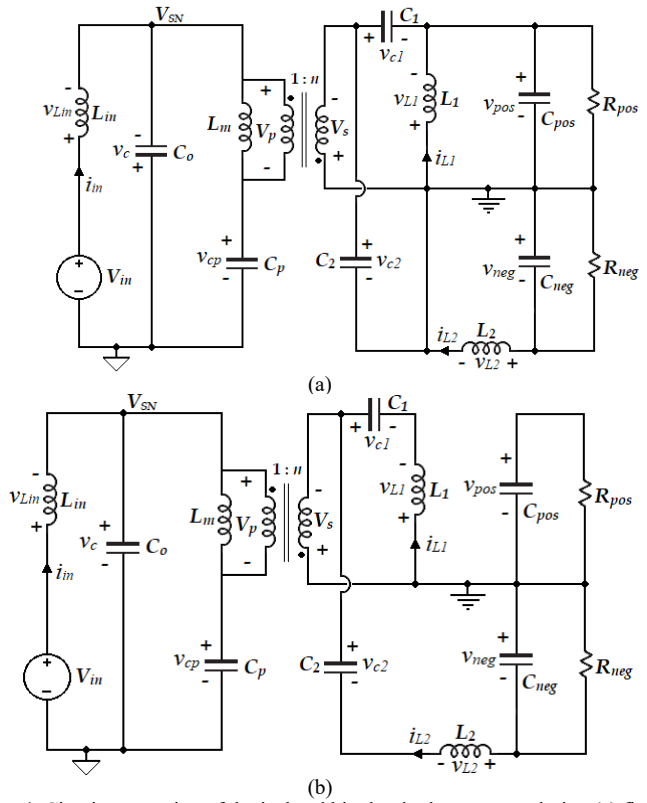

Fig. 4. Circuit connection of the isolated bipolar dc-dc converter during (a) first subinterval or D interval and (b) in second subinterval or (1-D) interval.

First subinterval or D interval ($0 < t < DT_S$)

$$v_{Lin} = V_{in} + v_c \tag{1}$$

$$v_p = -v_c - v_{cp} \tag{2}$$

$$v_s = -n\left(v_c + v_{cp}\right) \tag{3}$$

$$v_{L1} = -v_{pos} \tag{4}$$

$$v_{L1} = v_s + v_{c1} = -n\left(v_c + v_{cp}\right) + v_{c1} \tag{5}$$

$$v_{L2} = v_s + v_{c2} - v_{neg}$$

$$v_{L2} = -n\left(v_c + v_{cp}\right) + v_{c2} - v_{neg} \tag{6}$$

$$v_{L2} = -v_{neg} \tag{7}$$

In the second subinterval ($DT_S < t < T_S$) or (1-D) interval, the switches S_1 and S_2 are turned off and the diodes D_1 and D_2 are forward biased. The secondary side diodes D_3 and D_4 stop conducting. Now, the input inductor current i_{in} decreases with slope $(V_{in}\text{-}V_c)/L_{in}$ and energy is transferred to the capacitor C_o from the inductor L_{in}. Fig. 4 (b) shows the circuit schematic of the proposed converter in the second subinterval. The voltages across the input inductor L_{in}, primary and secondary windings of the HF transformer, output side inductors L_1 and L_2 are expressed in (8) - (12).

Second subinterval or (1-D) interval ($DT_S < t < T_S$)

$$v_{Lin} = V_{in} - v_c \tag{8}$$

$$v_p = v_c - v_{cp} \tag{9}$$

$$v_s = n\left(v_c - v_{cp}\right) \tag{10}$$

$$v_{L1} = v_s + v_{c1} = n\left(v_c - v_{cp}\right) + v_{c1} \tag{11}$$

$$v_{L2} = v_s + v_{c2} - v_{neg}$$

$$\text{or, } v_{L2} = n\left(v_c - v_{cp}\right) + v_{c2} - v_{neg} \tag{12}$$

B. Steady-State Analysis

Using small ripple approximation and volt-second balance of the input inductor L_{in}, the voltage V_c across the capacitor C_o can be obtained as

$$\left\langle v_{Lin} \right\rangle_{T_S} = D\left(V_{in} + V_c\right) + \left(1-D\right)\left(V_{in} - V_c\right) = 0$$

$$\Rightarrow V_c = \frac{1}{1-2D} V_{in} \tag{13}$$

From the volt-second balance of the magnetizing inductor L_m using (2) and (9), the voltage across the capacitor C_p is obtained as,

$$\left\langle v_p \right\rangle_{T_S} = D\left(-V_{cp} - V_c\right) + \left(1-D\right)\left(V_c - V_{cp}\right) = 0$$

$$\Rightarrow V_{cp} = \left(1-2D\right)V_c = V_{in} \tag{14}$$

From (7), (12), and (13), the volt-second balance of inductor L_2 yields

$$\left\langle v_{L2} \right\rangle_{T_S} = -DV_{neg} + \left(1-D\right)n\left(V_c - V_{in}\right) + \left(1-D\right)V_{c2} - \left(1-D\right)V_{neg} = 0$$

$$\text{or, } V_{neg} = \left(1-D\right)n\left(V_c - V_{in}\right) + \left(1-D\right)V_{c2} \tag{15}$$

Using (6), (12), and (13), the negative dc bus voltage V_{neg} is obtained as,

$$V_{neg} = -nD\left(V_c + V_{in}\right) + n\left(1-D\right)\left(V_c - V_{in}\right) + V_{c2}$$

$$= -nV_{in} + n\left(1-2D\right)V_c + V_{c2}$$

$$\text{or, } V_{neg} = V_{c2} \tag{16}$$

Putting the value of V_{neg} obtained from (16) in (15), V_{neg} can be expressed as,

$$V_{neg} = \frac{2n\left(1-D\right)}{1-2D} V_{in} \tag{17}$$

From the volt-second balance of the inductor L_1 using (4), (11), and (14), the expression for the positive dc bus voltage V_{pos} is obtained as

$$V_{pos} = \frac{2n\left(1-D\right)}{1-2D} V_{in} \tag{18}$$

From (17) and (18), it can be seen that the voltages of the positive and negative bus are equal, which form the bipolar dc bus at the output of the converter.

The waveforms of the switch node voltage (v_{SN}), the transformer primary voltage (v_p), and the secondary voltage (v_s) along with the gate switching signals of switch S_1, S_2 (G_{S1}, G_{S2}) are shown in Fig. 5 (a) for continuous conduction mode (CCM) of operation. The waveforms of the input current (i_{in}), current through switches S_1 and S_2 (i_{S1}, i_{S2}), current through diodes D_1 and D_2 (i_{D1}, i_{D2}), and primary winding current of the transformer (i_{prim}) is shown in Fig. 5 (b).

The conversion ratio (V_{pos}/V_{in} or V_{neg}/V_{in}) plot of the proposed converter (for n=0.5 and 1) is shown in Fig. 6. The gain plot of the SEPIC-Čuk derived bipolar converter presented in [12] is also plotted in Fig. 6, which shows that the proposed converter can provide higher gain. It can be also seen that a higher conversion ratio can be achieved by

increasing either the duty ratio (D) of the converter or the transformer turns-ratio n. With the increase in transformer turns-ratio, the gain at D=0 rises linearly as quantified in (18). It can be observed that the duty ratio of the converter has to be restricted below D=0.5 for proper operation.

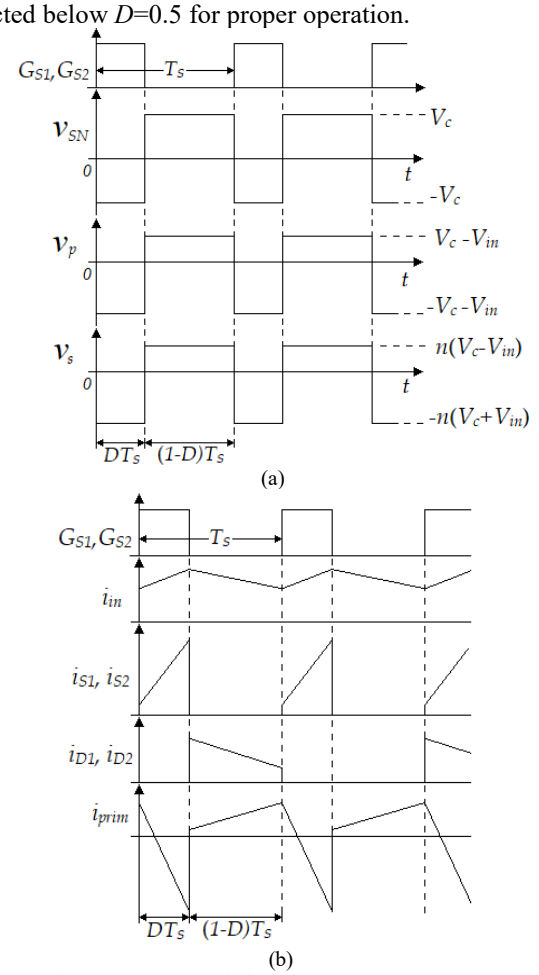

Fig. 5. Waveforms of the (a) switch node voltage (v_{SN}), transformer primary and secondary voltages (v_p and v_s) and (b) input current (i_{in}), switch current (i_{S1}, i_{S2}), diode current (i_{D1}, i_{D2}), and transformer primary current (i_{prim}) along with the gating signals G_{S1}, G_{S2}.

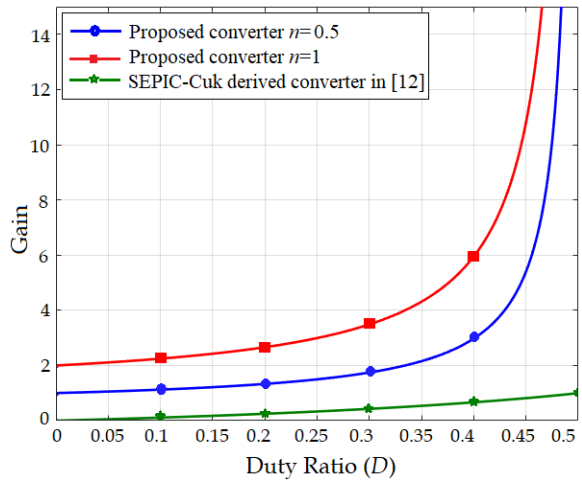

Fig. 6. Conversion ratio plot of the proposed converter with transformer turns-ratio n=0.5 and 1 and the SEPIC-Čuk derived bipolar converter in [12].

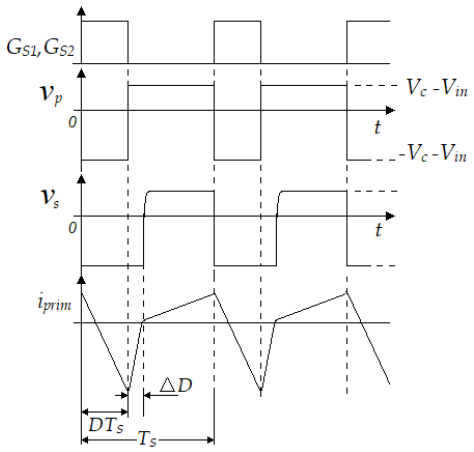

Fig. 7. Effect of finite leakage inductance of the transformer on the transformer primary and secondary voltages (v_p and v_s) and transformer primary current (i_{prim}).

C. Effect of Finite Leakage Inductance on Converter Operation

The operation of the proposed converter gets modified in presence of a finite leakage inductance of the HF transformer (L_{lkg}). A finite leakage inductance prevents instantaneous change in the primary current when the gate signals of the switches S_1 and S_2 are turned off. Due to the presence of the leakage inductance, the primary winding current (i_{prim}) takes finite time to rise when a positive voltage is applied across the primary winding [16]. This finite slope of i_{prim} reduces the duty cycle of the secondary voltage. The effective duty ratio (D_{eff}) of the secondary winding voltage can be expressed as

$$1 - D_{eff} = 1 - D - \Delta D$$

where ΔD is the loss of duty ratio due to the finite rising slope of the primary current. The waveforms of the primary and secondary winding voltages (v_p and v_s), primary winding current (i_p) along with the gate signals G_{S1} and G_{S2} are shown in Fig. 7, which depicts the effect of duty cycle loss.

D. Component Stress and Sizing of Passive Components

The value of input inductor L_{in}, output side inductors L_1, L_2 can be expressed in terms of their current ripple, switching time period T_S, and duty ratio D as:

$$L_{in} = \frac{V_{in} + V_c}{\Delta i_{in}} DT_S,\ L_1 = \frac{V_{pos}}{\Delta i_{L1}} DT_S,\ L_2 = \frac{V_{neg}}{\Delta i_{L2}} DT_S$$

The maximum voltages appearing across the switches and diodes are given below.

$$V_{S1} = V_{S2} = \frac{V_{in}}{1-2D},\ V_{D1} = V_{D2} = -\frac{V_{in}}{1-2D},\ V_{D3} = V_{D4} = -\frac{2nV_{in}}{1-2D}$$

E. Battery Discharge Restricting Capability

In dc marine ships or dc ferries that run on the power from BESSs, it is essential to have an efficient fault management strategy in order to isolate the fault and restrict the current from the battery bank from rapid discharge and to prevent it from feeding power to the fault. The proposed converter can play a major role in isolating the battery bank and restricting

rapid battery discharge. As the output side of the converter is isolated from the input side by the high frequency transformer, stopping the power transfer through the transformer can prevent discharge of the battery bank. This can be done by turning off the gate pulses of the switches S_1 and S_2. As the switching pulses are removed, the switch node voltage (v_{SN}) assumes a steady voltage equal to the input voltage. This results in a zero voltage appearing at the primary terminals of the transformer as the capacitor voltage V_{cp} is equal to V_{in}. Thus, power flow from primary to secondary winding is prevented. Also, the input current decays to zero, as zero voltage appears across its terminals.

V. Simulation Results

The proposed converter is simulated in MATLAB®/Simulink platform to verify its steady-state and dynamic behavior. The passive component parameters of the converter are given in Table I. A high frequency transformer with turns-ratio $n=N_s/N_p=1$ is selected. A 50-kW distribution system having ±750 V dc bus voltage with 400 V dc input is chosen for the simulations with a switching frequency of 10 kHz.

The switching cycle variations in the transformer primary and secondary voltages (v_p and v_s), transformer primary current i_{prim} along with gate signals G_{S1} and G_{S2} are shown in Fig. 8. The converter waveforms for transformer leakage inductance L_{lkg}=0.5 µH and L_{lkg}=15 µH are shown in Fig. 8 (a) and Fig. 8 (b), respectively. From Fig. 8, it is seen that the finite rising slope of the primary current reduces the duty cycle of the secondary voltage when the transformer leakage inductance is substantial. In a closed loop controlled system, the duty loss leads to an increase in the duty ratio of the switches S_1 and S_2 in order to compensate for the voltage loss at the output. As the duty ratio increases, the primary side capacitor voltage V_c increases, which leads to requirement of higher voltage rated switches. Thus, it is preferred to have a transformer leakage inductance as small as possible.

TABLE I.
Passive Component Parameters

Components	Attributes
L_{in}	600 µH
C_o	500 µF
L_1, L_2	1000 µH
C_p, C_1, C_2	500 µF
C_{pos}, C_{neg}	2000 µF

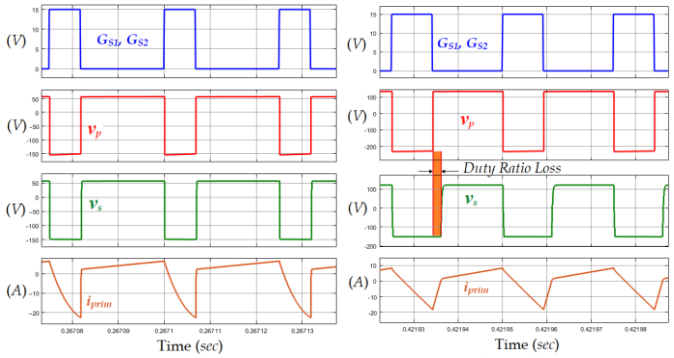

Fig. 8. Effect of transformer leakage inductance on the secondary winding voltage with leakage inductance of: (a) 0.5 µH and (b) 15 µH, depicting the effect of duty loss.

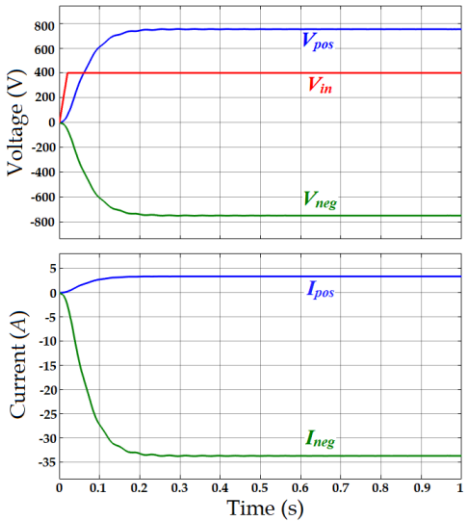

Fig. 9. Simulation waveforms of the positive and negative dc bus voltages (V_{pos}, V_{neg}), input voltage (V_{in}), and load currents of the positive and negative buses (I_{pos}, I_{neg}) for ±750 V reference with unequal loading.

A. Steady-State Operation in Closed Loop Control with Unequal Loading

A closed loop control is implemented using a type-II [17] controller with the isolated bipolar dc-dc converter. To test the operation of the converter in closed loop and its ability to regulate the bipolar dc bus voltages at their reference voltages, it is tested with severe unequal loading condition and dynamic load variation. The steady-state operation of the converter with unequal loading is shown in Fig. 9 with the converter startup process. The reference for the bipolar dc bus voltages is ±750 V. The load resistances are 222.22 Ω and 22.22 Ω for the positive and negative dc bus, respectively. A ramp up time of 20 ms is provided for the dc source. From Fig. 9, it is seen that both the positive and negative dc bus voltages settle at the reference values of 750 V and -750 V, respectively. The load currents of the positive and negative buses settle at 3.375 A and -33.75 A, respectively according to the load resistances.

B. Dynamic Operation with Closed Loop Control

The isolated bipolar converter is tested for load step up and load step down changes to verify the dynamic performance of the converter. The positive dc bus resistance is kept at 40 Ω while the negative dc bus resistance is kept at 22.22 Ω (parallel connection of 40 Ω and 50 Ω) during converter startup. At t=0.9 sec, a 50-Ω load is connected to the positive dc bus and at t=1.3 sec, the 50-Ω load is disconnected from the negative dc bus. The simulation results for the dynamic operation of the converter are shown in Fig. 10. This figure shows that the converter is able to regulate its outputs at ±750 V after the step up and step down load changes and sustain the bus voltages at their reference values even under load unbalance condition.

C. Battery Discharge Restricting Capability During Fault

The capability of the proposed converter to restrict the battery current from rapid discharge at the event of short circuit fault is simulated. A pole-to-pole short circuit fault is created at t=0.9 s with the fault resistance being 0.2 Ω.

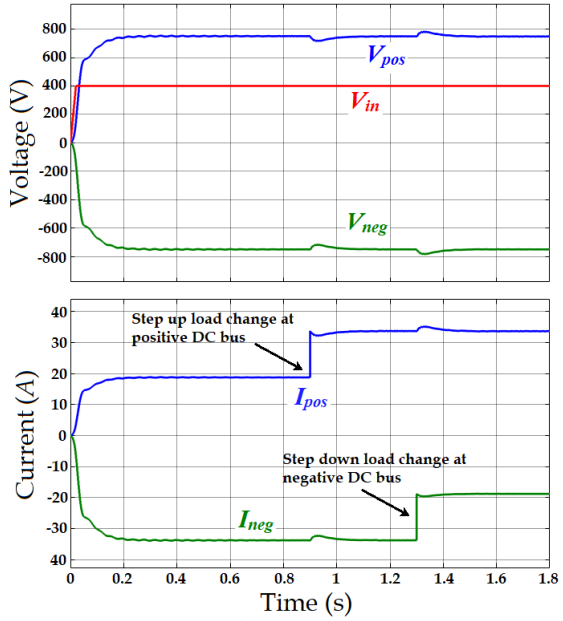

Fig. 10. Dynamic performance of the isolated bipolar converter showing the waveforms of positive and negative dc bus voltages (V_{pos}, V_{neg}), input voltage (V_{in}), and load currents of the positive and negative buses (I_{pos}, I_{neg}) at the event of step up load change at the positive dc bus (at t=0.9 s) and step down load change at the negative dc bus (t=1.3 s).

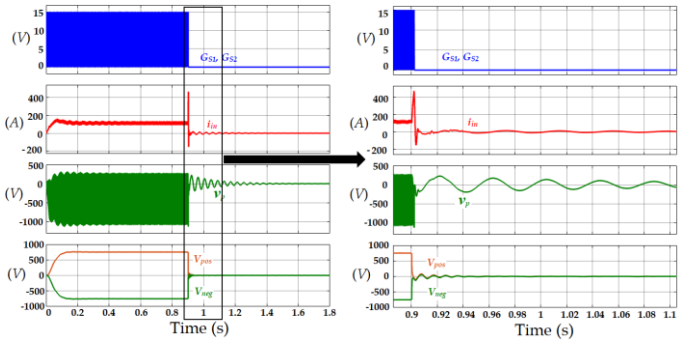

Fig. 11. Simulation waveforms of the input current (i_{in}), transformer primary voltage (v_p), positive and negative dc bus voltage (V_{pos}, V_{neg}) at the event of pole to pole short circuit fault (at t=0.9 s) and gate pulse removal at t=0.902 s.

Assuming a proper fault detection algorithm exists, the gate pulses are withdrawn after 2 ms. Fig. 11 shows the simulation results. It can be observed that the primary voltage of the transformer decays to zero after the gate switching signals ate withdrawn. Also, the input current becomes zero, which indicates that the battery doesn't feed power to the fault.

VI. Conclusion

In this paper, an isolated bipolar dc-dc converter has been presented. This converter is intended to act as the interface between the battery energy storage system and dc distribution system in marine vessels. The detailed steady-state analysis of the proposed converter is presented. The relation between its input and output variables are deduced and the effect of finite transformer leakage inductance of the transformer on the converter performance is shown. The capability of the converter to restrict power flow from the BESS at the event of short circuit bus fault is explained. A suitable closed loop controller is developed, which enables the converter to regulate its output voltages at the reference values. The dynamic performance of the converter has been tested by load step up and step down changes in the positive and negative bus, respectively. The capability of restricting battery discharge current during short circuit fault has also been verified by simulation.

References

[1] ABB, "The step forward onboard dc grid," technical report, 2014 [Online].

[2] W. Koczara and G. Iwanski, Power electronics for renewable and distributed energy systems, ch. variable-speed power generation. Springer, 2013.

[3] F. D. Kanellos, "Optimal power management with ghg emissions limitation in all-electric ship power systems comprising energy storage systems," *IEEE Trans. Power Sys.*, vol. 29, pp. 330–339, Jan. 2014.

[4] J. Hou; J. Sun; H. F. Hofmann, "Mitigating power fluctuations in electric ship propulsion with hybrid energy storage system: design and analysis," Early Access Article, *IEEE Journal of Oceanic Engineering* , DOI: 10.1109/JOE.2017.2674878.

[5] E. Skjong, E. Rodskar, M. Molinas, T. A. Johansen and J. Cunningham, "The marine vessel's electrical power system: from its birth to present day," *Proceedings of the IEEE*, vol. 103, no. 12, pp. 2410-2424, Dec. 2015.

[6] Corvus Energy, "CASE STUDY: norled as, mf ampere, ferry – webydo," technical report, 2015.

[7] "IEEE recommended practice for 1 kv to 35 kv medium-voltage dc power systems on ships," IEEE Std 1709-2010, pp. 1–54, Nov 2010.

[8] S. Wang, Z. Zheng, Y. Li and L. Peng, "A modular dc solid state transformer for future onboard dc grid," in *Proc. International Conference on Electrical Systems for Aircraft, Railway, Ship Propulsion and Road Vehicles & International Transportation Electrification Conference* (ESARS-ITEC), Toulouse, 2016, pp. 1-6.

[9] F. D. Kanellos, G. J. Tsekouras and J. Prousalidis, "Onboard dc grid employing smart grid technology: challenges, state of the art and future prospects," *IET Electr. Syst. Transp*., vol. 5, no. 1, pp. 1-11, Mar. 2015

[10] J. F. Hansen and F. Wendt, "History and state of the art in commercial electric ship propulsion, integrated power systems, and future trends," *Proceedings of the IEEE*, vol. 103, no. 12, pp. 2229-2242, Dec. 2015.

[11] R. R. Chan, L. Chua and T. Tjahjowidodo, "Enabling technologies for sustainable all – electric hybrid vessels," in *Proc. IEEE Int. Conf. on Sustainable Energy Technologies*, Nov. 14-16, 2016, pp. 401-406.

[12] M. B. Ferrera, S. P. Litrán, E. Durán Aranda and J. M. Andújar Márquez, "A converter for bipolar dc link based on sepic-cuk combination," *IEEE Trans. Power Electron.*, vol. 30, no. 12, pp. 6483-6487, Dec. 2015.

[13] F. Wang, Z. Lei, X. Xu and X. Shu, "Topology deduction and analysis of voltage balancers for dc microgrid," *IEEE J. Emerg. Sel. Topics Power Electron*, vol. 5, no. 2, pp. 672-680, Jun. 2017.

[14] X. Zhang and C. Gong, "Dual-buck half-bridge voltage balancer," *IEEE Trans. on Indus. Electron.*, vol. 60, no. 8, pp. 3157-3164, Aug. 2013.

[15] R. W. Erickson, D. Maksimović, Fundamentals of power electronics, New York, NY, USA:Springer Science+Business Media, LLc, pp. 150, 2001, ch. 6.2.

[16] V. Vlatkovic, J. A. Sabate, R. B. Ridley, F. C. Lee and B. H. Cho, "Small-signal analysis of the phase-shifted PWM converter," *IEEE Transactions on Power Electronics*, vol. 7, no. 1, pp. 128-135, Jan 1992.

[17] A. Ghosh, S. Banerjee, M. K. Sarkar and P. Dutta, "Design and implementation of type-II and type-III controller for dc–dc switched-mode boost converter by using K-factor approach and optimisation techniques," *IET Power Electronics*, vol. 9, no. 5, pp. 938-950, 2016.